Sensors & Transducers, Vol. 196, Issue 1, January 2016, pp. 57-68

Sensors & Transducers

http://www.sensorsportal.com

Improving Vibration Energy Harvesting Using Dynamic Magnifier

[1] Almuatasim Alomari, [1] Ashok Batra and [2] C. R. Bowen

[1] Department of Physics, Chemistry and Mathematics (Materials Science Group), Alabama A&M University, Normal (Huntsville), AL 35762 USA

[2] Department of Mechanical Engineering, University of Bath, Bath, BA2 7AY, UK

Received: 17 December 2015 /Accepted: 18 January 2016 /Published: 31 January 2016

Abstract: This paper reports on the design and evaluation of vibration-based piezoelectric energy-harvesting devices based on a polyvinylidene fluoride unimorph cantilever beam attached to the front of a dynamic magnifier. Experimental studies of the electromechanical frequency response functions are studied for the first three resonance frequencies. An analytical analysis is undertaken by applying the chain matrix in order to predict output voltage and output power with respect to the vibration frequency. The proposed harvester was modeled using MATLAB software and COMSOL multi-physics to study the mode shapes and electrical output parameters. The voltage and power output of the energy harvester with a dynamic magnifier was 2.62 V and 13.68 μW, respectively at the resonance frequency of the second mode. The modeling approach provides a basis to design energy harvesters exploiting dynamic magnification for improved performance and bandwidth. The potential application of such energy harvesting devices in the transport sector include autonomous structural health monitoring systems that often include embedded sensors, data acquisition, wireless communication, and energy harvesting systems. *Copyright © 2016 IFSA Publishing, S. L.*

Keywords: Harvesting, Piezoelectric, Modeling, Resonance, MATLAB, COMSOL.

1. Introduction

In recent years there has been an increasing interest in employing piezoelectric energy harvesters (PEHs) in applications such as autonomous low-power electronics and wireless sensors [1-3]. Traditionally, the capture of ambient vibrational energy from the surrounding environment is an effective and popular technique to provide small amount of power (μW to mW) for low-energy electronics [4-5]. Piezoelectric harvesters based on cantilever configurations play a prominent role in this area, which convert mechanical energy into electrical energy. The devices can be considered as complex multi-physics systems requiring advanced methodologies to maximize their performance and convert ambient vibrations into useable electrical power [6]. Piezoelectric materials are attracting interest for applications such as harvesting since they have strong electro-mechanical coupling and a high frequency response [7]. Conventional piezoelectric energy harvester devices operate as linear vibration resonators which are often limited to the capture of low vibration amplitudes that are close to the resonance frequency of the harvester [8]. However, energy harvesters with dynamic magnifier configurations are of interest due to their ability to work at different resonance frequencies as well as magnify the bandwidth of the harvester. One of the simplest configurations of a conventional piezoelectric energy harvester (CPEH) devices is a tip mass attached at the front of a piezoelectric cantilever energy harvester, as shown in Fig. 1 (a).

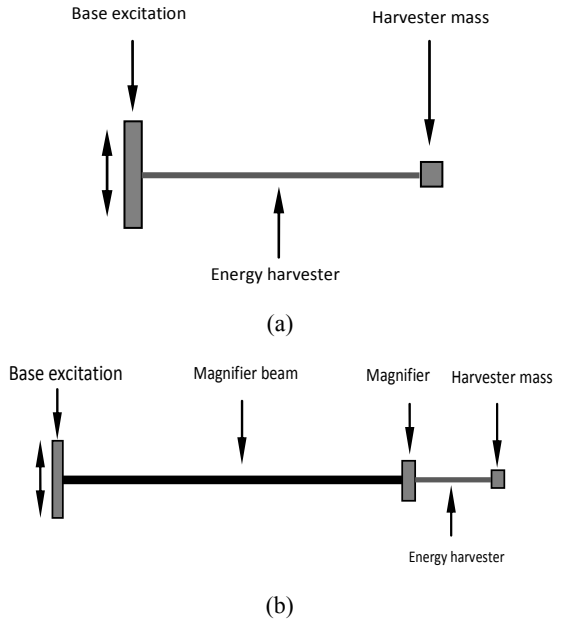

Fig. 1. (a) Conventional Piezoelectric Energy harvester with mass (CPEH); (b) Energy harvester with dynamic magnifier and mass (EHDM).

In order to enhance the maximum output power and operational bandwidth of piezoelectric energy harvesters, researchers have developed a variety of techniques based on, varying shape of structure beam using an L-shaped flexible structure [9-11], adding an additional impendence between the piezoelectric harvester and load resistance [12-15], using dual-mass systems [16], changing the cross-section of a dynamic magnifier [17] and using an energy harvester with a dynamic magnifier (EHDM) as shown in Fig. 1(b). The use of EHDM has been successful in amplifying the energy harvesting efficiency and widening the bandwidth of the device. A variety of EHDM models have been developed with the purpose of understanding the system and enhancing the device efficiency. Zhou, *et al.* developed a novel piezoelectric energy harvester with a multi-mode dynamic magnifier, which is capable of significantly increasing the bandwidth and the energy harvested from ambient vibrations [18]. Aladwani, *et al.* [19] and Aldraihem, *et al.* [20] have studied the piezoelectric harvester with a dynamic magnifier consisting of a spring-mass both experimentally and analytically where the system was able to amplify the electrical power output and enhanced the bandwidth of the harvester. Lee, *et al.* have investigated an innovative design platform of a piezoelectric energy harvester termed a segment-type energy harvester experimentally and analytically using finite element method (FEM) where the system showed excellent performance and generated sufficient power to operate a temperature wireless sensor [21]. A bimorph beam with a tip mass attached at the front of a dynamic magnifier was modeled and studied by Vasic, *et al.* where the numerical results showed that electric power produced by the harvesting beam is amplified for efficient energy harvesting over a broader frequency range [22]. The potential application of such energy harvesting devices in the transport sector include autonomous structural health monitoring systems in trains or aerospace structures that typically include embedded sensors, data acquisition, wireless communication, and energy harvesting systems.

According to literature, limited research has examined the modeling of a unimorph beam attached at the front end of a magnifier with mass using the chain matrix technique for low electronic devices applications. The reason of choosing the chain matrix technique is that the model enables examination of the various electrical and mechanical boundary conditions by breaking the structure into elementary elements that can be readily adapted to represent different configurations of a dynamic magnifier energy harvester [22]. In this study, a mass was attached at the front of unimorph piezoelectric energy harvester to act as a conventional piezoelectric energy harvester, Fig. 1(a). A mass was then positioned between the copper beam and conventional piezoelectric energy harvester to form a dynamic magnifier energy harvester with mass (EHDM), as in Fig. 1(b). This research examined the influence of attaching a mass at the front of unimorph beam with dynamic magnifier on harvested power and bandwidth of the device. Analytical simulation of the harvesting system was carried out using MATLAB and finite element analysis was utilized for determination of mode shapes using COMSOL.

2. Mathematical Analysis of Dynamic Magnifier Model

2.1. Unimorph Beam

The piezoelectric unimorph beam in this study consists a piezoelectric layer which is sandwiched between two conducting electrodes and positioned on the top of shim layer, as shown in Fig. 2.

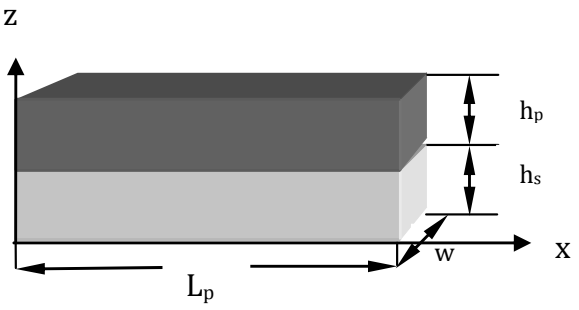

Fig. 2. Piezoelectric unimorph beam.

The length and the width of the unimorph are denoted by L_p and w, respectively. The thickness of the piezoelectric layer and shim layer are h_p and h_s, respectively. The expressions of the bending moment M and the transverse shear force F relative to the

position x and according to the piezoelectric voltage V are written as [22]:

$$M = -K_u \frac{\partial^2 u}{\partial x^2} + N_u V, \quad (1)$$

$$F = \frac{\partial M}{\partial x} = -K_u \frac{\partial^3 u}{\partial x^3}, \quad (2)$$

where K_u is the effective bending rigidity of the entire unimorph beam, N_u is the constant of the electro-mechanical conversion.

Both previous quantities are defined for the unimorph beam in Fig. 2 mathematically as [23-25]:

$$K_u = \frac{1}{12} w\left(4E_s h_s^3 + E_p h_p^3 + 3E_s h_s h_p (2h_s + h_p)\right), \quad (3)$$

$$N_u = -\frac{w d_{31} E_p h_s}{8h_p}\left(h_s + 2h_p\right), \quad (4)$$

where E_s, E_p are the Young's modulus of the shim layer and piezoelectric material, respectively, d_{31} is piezoelectric strain coefficient of the piezoelectric material.

The equation of the motion of the elastic unimorph beam is given as:

$$K_u \frac{\partial^4 u}{\partial x^4} + w(\rho_s h_s + \rho_p h_p)\frac{\partial^2 u}{\partial t^2} = 0, \quad (5)$$

where ρ_s, ρ_p are the densities of the shim and piezoelectric layer, respectively. By considering a harmonic mode, the general solution of displacement in Eq. (5) can be written as [26]:

$$u = \alpha_1 \cos \lambda_u x + \alpha_2 \sin \lambda_u x + \alpha_3 \cosh \lambda_u x + \alpha_4 \sinh \lambda_u x, \quad (6)$$

where $\alpha_1 - \alpha_4$ are the coefficients determined from the boundaries conditions and λ_u is the wave number:

$$\lambda_u = \left(\frac{\overline{\rho}_u}{K_u}\omega^2\right)^{1/4}, \quad (7)$$

where ω is the vibration frequency and $\overline{\rho}_u$ is the linear mass:

$$\overline{\rho}_u = w(\rho_s h_s + \rho_p h_p) \quad (8)$$

In order to model this element, we have established a relationship between the bending moment denoted M_1, the rotational velocity Φ_1, the transverse shear force F_1, and the vertical velocity U_1 at the position x=0 according to these same quantities (M_2, Φ_2, F_2, U_2) at the position x=L_p as shown in Fig. 3.

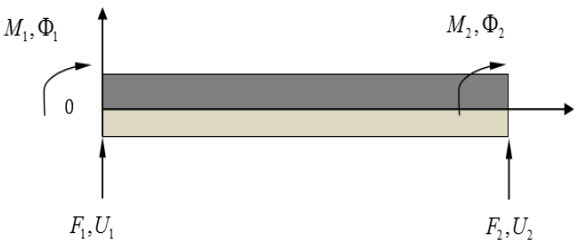

Fig. 3. Bending moments M_1 M_2, transverse shear forces F_1 F_2, vertical velocities U_1 U_2 and rotational velocities $\Phi_1\Phi_2$ at the ends. Same here – narrow arrow ends otherwise it dominated the image.

By taking into account the following boundary conditions of the bending moments and the transverse shear efforts at the ends:

$$F_1 = F\big|_{x=0} \text{ and } M_1 = M\big|_{x=0} \quad (9)$$

$$F_2 = -F\big|_{x=L_p} \text{ and } M_2 = -M\big|_{x=L_p} \quad (10)$$

Velocities at the ends of the beam corresponding to linear displacements and rotation are defined by [27]:

$$U_1 = \frac{\partial u}{\partial t}\big|_{x=0} \text{ and } \Phi_1 = -\frac{\partial^2 u}{\partial t \partial x}\big|_{x=0} \quad (11)$$

$$U_2 = \frac{\partial u}{\partial t}\big|_{x=L_p} \text{ and } \Phi_2 = -\frac{\partial^2 u}{\partial t \partial x}\big|_{x=L_p} \quad (12)$$

matrix relations can be establish as shown in Eq. (13) and Eq. (14).

$$\begin{bmatrix} U_1 \\ \Phi_1 \\ U_2 \\ \Phi_2 \end{bmatrix} = j\omega \begin{bmatrix} 1 & 0 & 1 & 0 \\ 0 & -\lambda_u & 0 & -\lambda_u \\ c_b & s_u & m_b & n_u \\ \lambda_u s_u & -\lambda_u c_u & -\lambda_u n_u & -\lambda_u m_u \end{bmatrix} \begin{bmatrix} \alpha_1 \\ \alpha_2 \\ \alpha_3 \\ \alpha_4 \end{bmatrix} \quad (13)$$

and

$$\begin{bmatrix} F_1 \\ M_1 \\ F_2 \\ M_2 \end{bmatrix} = j\omega \begin{bmatrix} 0 & -\lambda_u^3 & 0 & \lambda_u^3 \\ -\lambda_u^2 & 0 & \lambda_u^2 & 0 \\ -\lambda_u^3 s_u & \lambda_u^3 c_u & \lambda_u^3 n_u & -\lambda_u^3 m_u \\ \lambda_u^2 c_u & \lambda_u^2 s_u & -\lambda_u^2 m_u & -\lambda_u^2 n_u \end{bmatrix} \begin{bmatrix} \alpha_1 \\ \alpha_2 \\ \alpha_3 \\ \alpha_4 \end{bmatrix}, \quad (14)$$

where $c_u = \cos \lambda_u L_p$, $s_u = \sin \lambda_u L_p$,

$m_u = \cosh \lambda_u L_p$, $n_u = \sinh \lambda_u L_p$.

By eliminating the coefficient α_1 to α_4, we establish a 4×4 matrix relationship (Eq. (15)) connecting the efforts and velocities of one end of the beam (x = 0) to the other (x = L_P) including the voltage V.

$$\begin{bmatrix} F_1 \\ M_1 \\ U_1 \\ \Phi_1 \end{bmatrix} = \Gamma^{L_p} \begin{bmatrix} -F_2 \\ -M_2 \\ U_2 \\ \Phi_2 \end{bmatrix} + \Pi^{L_p} V, \quad (15)$$

where Γ^{L_p} is called the 4×4 chain matrix, defined by:

$$\Gamma^{L_p} = \frac{1}{2} \begin{bmatrix} m_u + c_u & -\lambda_u (n_u - s_u) & \frac{K_u \lambda_u^3 (n_u + s_u)}{j\omega} & \frac{K_u \lambda_u^2 (m_u - c_u)}{j\omega} \\ \frac{-(n_u + s_u)}{\lambda_u} & m_u + c_u & \frac{-K_u \lambda_u^2 (m_u - c_u)}{j\omega} & \frac{K_u \lambda_u (n_u - s_u)}{j\omega} \\ \frac{j\omega (n_u - s_u)}{K_u \lambda_u^3} & \frac{-j\omega (m_u - c_u)}{K_u \lambda_u^2} & m_u + c_u & \frac{(n_u + s_u)}{\lambda_u} \\ \frac{j\omega (m_u - c_u)}{K_u \lambda_u^2} & \frac{-j\omega (n_u + s_u)}{K_u \lambda_u} & \lambda_u (n_u - s_u) & m_u + c_u \end{bmatrix} \quad (16)$$

and Π^{Lp} is a matrix 1×4 defined by:

$$\Pi^{L_p} = \begin{bmatrix} \frac{N_u \lambda_u (n_u - s_u)}{2} \\ N_u - \frac{N_u (m_u + c_u)}{2} \\ \frac{j\omega N_u (m_u - c_u)}{2K_u \lambda_u^2} \\ \frac{j\omega N_u (n_u + s_u)}{2K_u \lambda_u} \end{bmatrix} \quad (17)$$

2.2. Magnifier Beam

For a magnifier beam (shown in Fig. 1), the effective bending rigidity K_m can be written as:

$$K_m = \frac{w h_m^3}{12 s_{m11}} \quad (18)$$

The equation of the motion of the magnifier beam is given as:

$$K_m \frac{\partial^4 u}{\partial x_1^4} + w \rho_m h_m \frac{\partial^2 u}{\partial t^2} = 0 \quad (19)$$

By considering a harmonic mode, the relation connecting the bending moments M_1 M_2, transverse shear forces F_1 F_2 and velocities of one end of the beam to the other end is obtained in a similar way to the previous case as in Eqs. (9-14) but the electro-mechanical constant is not used.

$$\begin{bmatrix} F_1 \\ M_1 \\ U_1 \\ \Phi_1 \end{bmatrix} = \Gamma^{L_m} \begin{bmatrix} -F_2 \\ -M_2 \\ U_2 \\ \Phi_2 \end{bmatrix}, \quad (20)$$

where Γ^{L_m} is the 4×4 chains matrix, defined by:

$$\Gamma^{L_m} = \frac{1}{2} \begin{bmatrix} m_L + c_L & -\lambda_m (n_L - s_L) & \frac{K_m \lambda_m^3 (n_L + s_L)}{j\omega} & \frac{K_m \lambda_m^2 (m_L - c_L)}{j\omega} \\ \frac{-(n_L + s_L)}{\lambda_L} & m_L + c_L & \frac{-K_m \lambda_m^2 (m_L - c_L)}{j\omega} & \frac{K_m \lambda_m (n_L - s_L)}{j\omega} \\ \frac{j\omega (n_L - s_L)}{K_m \lambda_m^3} & \frac{-j\omega (m_L - c_L)}{K_m \lambda_m^2} & m_L + c_L & \frac{(n_L + s_L)}{\lambda_m} \\ \frac{j\omega (m_L - c_L)}{K_m \lambda_m^2} & \frac{-j\omega (n_L + s_L)}{K_m \lambda_m} & \lambda_m (n_L - s_L) & m_L + c_L \end{bmatrix} \quad (21)$$

where $c_L = \cos \lambda_m L_m$, $s_L = \sin \lambda_m L_m$, $m_L = \cosh \lambda_m L_m$, $n_L = \sinh \lambda_m L_m$.

$$\lambda_m = \left(\frac{\bar{\rho}_m}{K_m} \omega^2 \right)^{1/4} \quad (22)$$

and the linear mass density:

$$\bar{\rho}_m = w \rho_m h_m \quad (23)$$

3. Composition of the Model

In the general case, the determination of the complete model of a particular device structure is undertaken by assembling simple elements that are

characterized by their chain matrix and their electro-mechanical conversion matrix thereby revealing the electrical variables (V and I). Thus, if we consider the particular case of the structure represented in Fig. 1, the separation of the system into simple elements is made in Fig. 4. The chain relation of each element of the harvester is:

$$\text{Section 1:} \begin{bmatrix} F_1 \\ M_1 \\ U_1 \\ \Phi_1 \end{bmatrix} = \Gamma^{Lm} \begin{bmatrix} -F_{21} \\ -M_{21} \\ U_{21} \\ \Phi_{21} \end{bmatrix}, \tag{24}$$

$$\text{Section 2:} \begin{bmatrix} F_{22} \\ M_{22} \\ U_{22} \\ \Phi_{22} \end{bmatrix} = \Gamma^{Lp} \begin{bmatrix} -F_3 \\ -M_3 \\ U_3 \\ \Phi_3 \end{bmatrix} + \Pi^{L_p} V, \tag{25}$$

where Γ^{Lm} is the chain matrix of the magnifier, Γ^{Lp} is the chain matrix of the energy harvesting beam with piezoelectric elements and the mass m_1 at the end of the magnifier and mass m_2 at the end of the harvester beam are taken into account with chain matrices Γ^{m1} and Γ^{m1}, respectively.

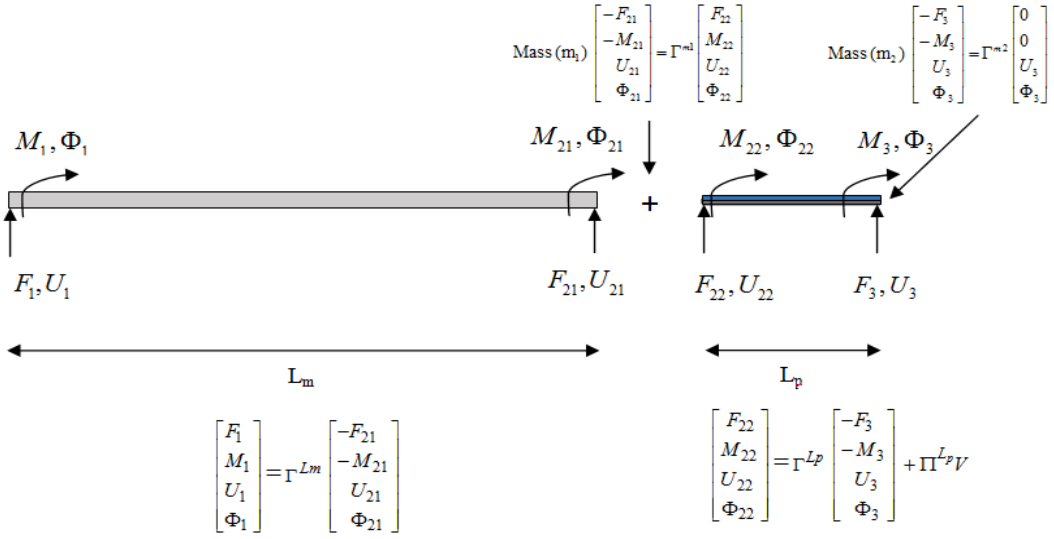

Fig. 4. Simple cutting elements of the energy harvester with the dynamic magnifier.

$$\begin{bmatrix} -F_{21} \\ -M_{21} \\ U_{21} \\ \Phi_{21} \end{bmatrix} = \Gamma^{m1} \begin{bmatrix} F_{22} \\ M_{22} \\ U_{22} \\ \Phi_{22} \end{bmatrix}, \begin{bmatrix} -F_3 \\ -M_3 \\ U_3 \\ \Phi_3 \end{bmatrix} = \Gamma^{m2} \begin{bmatrix} 0 \\ 0 \\ U_3 \\ \Phi_3 \end{bmatrix} \tag{26}$$

The expression of the two mass matrices is:

$$\Gamma^{m1} = \begin{bmatrix} 1 & 0 & j\omega m_1 & 0 \\ 0 & 1 & 0 & 0 \\ 0 & 0 & 1 & 0 \\ 0 & 0 & 0 & 0 \end{bmatrix}, \Gamma^{m2} = \begin{bmatrix} 1 & 0 & j\omega m_2 & 0 \\ 0 & 1 & 0 & 0 \\ 0 & 0 & 1 & 0 \\ 0 & 0 & 0 & 0 \end{bmatrix} \tag{27}$$

Considering that the excitation at the fixed end of the harvester is a sinusoidal excitation, A_{ext}, the boundary conditions at the embedded end: $U_1 = \frac{A_{ext}}{j\omega}$ and $\Phi_1 = 0$, and at the free end: $F_3 = 0$ and $M_3 = 0$. The continuity of the mechanical quantities at the junction of the sections enables the matrix relation of the complete energy harvester with magnifier to be:

$$\begin{bmatrix} F_1 \\ M_1 \\ \frac{A_{ext}}{j\omega} \\ 0 \end{bmatrix} = \Gamma^{Lm}\,\Gamma^{m1}\,\Gamma^{Lp}\,\Gamma^{m2} \begin{bmatrix} 0 \\ 0 \\ U_3 \\ \Phi_3 \end{bmatrix} + \Gamma^{Lm}\,\Gamma^{m1}\,\Pi^{L_p} V, \tag{28}$$

$$\Gamma^{har} = \Gamma^{Lm}\,\Gamma^{m1}\,\Gamma^{Lp}\,\Gamma^{m2} = \begin{bmatrix} \Gamma_1^{har} & \Gamma_2^{har} \\ \Gamma_3^{har} & \Gamma_4^{har} \end{bmatrix}, \tag{29}$$

$$\Pi^{har} = \Gamma^{Lm}\,\Gamma^{m1}\,\Pi^{L_p} = \begin{bmatrix} \Pi_1^{har} \\ \Pi_2^{har} \end{bmatrix} \tag{30}$$

We can extract two matrices relations Eq. (31) and Eq. (32) from Eq. (28):

$$\begin{bmatrix} F_1 \\ M_1 \end{bmatrix} = \Gamma_2^{har} \begin{bmatrix} U_3 \\ \Phi_3 \end{bmatrix} + \Pi_1^{har} V, \tag{31}$$

$$\begin{bmatrix} \frac{A_{ext}}{j\omega} \\ 0 \end{bmatrix} = \Gamma_4^{har} \begin{bmatrix} U_3 \\ \Phi_3 \end{bmatrix} + \Pi_2^{har} V \quad (32)$$

This second relation Eq. (32) enables the velocities at the end of the harvester beam to be calculated:

$$\begin{bmatrix} U_3 \\ \Phi_3 \end{bmatrix} = \left(\Gamma_4^{har}\right)^{-1} \begin{bmatrix} \frac{A_{ext}}{j\omega} \\ 0 \end{bmatrix} - \left(\Gamma_4^{har}\right)^{-1} \Pi_2^{har} V \quad (33)$$

The velocity Φ_3 can be expressed as:

$$\Phi_3 = [\left(\Gamma_4^{har}\right)^{-1}]_{21} \frac{A_{ext}}{j\omega} - [\left(\Gamma_4^{har}\right)^{-1} \Pi_2^{har}]_2 V, \quad (34)$$

$$\Phi_3 = A \frac{A_{ext}}{j\omega} - BV, \quad (35)$$

where $A = [\left(\Gamma_4^{har}\right)^{-1}]_{21}$ and $B = [\left(\Gamma_4^{har}\right)^{-1} \Pi_2^{har}]_2$

3.1. Electrical output Parameters

For calculation of the electrical output power of the energy harvester with a magnifier, firstly the electric current I is related to electric displacement D_3:

$$I = \int_A \frac{\partial D_3}{\partial t} dA_e, \quad (36)$$

where A_e is the area of the electrodes. The integration of Eq. (38) gives Eq. (39) [26]:

$$I = j\omega C_p V - N_u(\Phi_{22} - \Phi_3), \quad (37)$$

where C_p is the internal electrode capacitance of the piezoelectric layers, and is given by [27]

$$C_p = \frac{\varepsilon_{33}^T L_p w}{h_p} \quad (38)$$

The boundary condition imposed leads to $\Phi_{22} = 0$. If we consider a resistive load R connected at the electrodes of the piezoelectric layers, the voltage V can be expressed as:

$$V = -\frac{RN}{1 + j\omega RC_p} \Phi_3 \quad (39)$$

Eq. (35) provides an additional relationship between voltage and velocity Φ_3, thus relation Eq. (39) can be expressed as:

$$V = \frac{-RN_b A}{1 + j\omega RC_o - RN_b B} \frac{A_{ext}}{j\omega} \quad (40)$$

Finally, the expression of the output power is:

$$P = \frac{VV^*}{R} \quad (41)$$

4. Results and Discussion

4.1. Experimental Design Results and Analysis

In this section, we present both theoretical and experimental results of:

1) A conventional piezoelectric energy harvester with mass;

2) An energy harvester with dynamic magnifier and mass (EHDM).

Energy harvesting measurements were carried out initially by attaching a mass at the front of a commercial polyvinylidene fluoride (PVDF) unimorph cantilever beam in the configuration shown in Fig. 1(a). The second configuration involved attaching the polyvinylidene fluoride (PVDF) unimorph cantilever with mass at the front of copper cantilever beam with magnifier end-mass, as shown in Fig. 1(b). Both devices were then connected to a shaker system. The dimensions, electrical, mechanical properties of cantilever beams and magnifier end mass are shown in Table 1. A parametric study was undertaken using the experimental setup shown in Fig. 5.

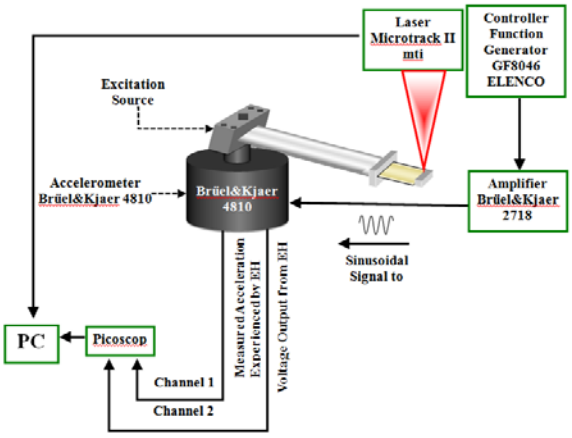

Fig. 5. Schematic diagram of the experimental set-up.

Fig. 6 shows the frequency response functions of output voltage and average output power for a CPEH and EHDM. It can be shown from Fig. 6 that there are three mode shapes of each proposed system, the blue circle line which represents the experimental results of CPEH has one peak at each mode shape, while the red circle line which represents the experimental results EHDM has two peaks at each

mode shape. The output voltage and the average output power of EHDM is larger than the CPEH and reached the maximum value at resonance frequencies of the first three modes. The energy harvesting bandwidth at every resonance frequency of the harvesting beam is widened in the EHDM configuration. It is convenient here to mention that the values of resonance frequency at 31 Hz and at 43 Hz will be of particular interests in this study due to high electrical output values. Fig. 7 and Fig. 8 show the experimental and theoretical data of the output voltage and average power for the conventional piezoelectric energy harvester and the EHDM, respectively; data is at a load resistance of 500 kΩ. It can be observed that the output voltage and average power in both cases have a good agreement between experiment and chain modeling. The resonance frequencies, output voltage, and average power of the first three modes for the CPEH and the EHDM from the graphs in Fig. 7 and Fig. 8 are summarized in Table 2.

Fig. 9 shows the output voltage and average power for EHDM at a range of load resistances, R_L, from 100 Ω to 10 MΩ. It can be seen from Fig. 9(a) that the output voltage increases with increasing R_L and the resonance frequency of the EHDM harvester depends on the external load resistance R_L. Moreover, the output power has a good agreement between experiment and modeling with an optimum power at the condition $2\pi \cdot f \cdot R_L \cdot C_p = 1$, where C_p is capacitance of the unimorph cantilever beam element (2.7 nF). The maximum peak of power can be observed between 300-600 kΩ; see Fig. 9(b).

Table 1. Properties of cantilever beams investigated. Magnifier end mass=5 g, unimorph end mass=1 g.

Type of beam	Magnifier beam	Piezoelectric unimorph cantilever beam	
	Copper	PVDF layer	Shim layer
Length (m)	L_m=0.150	L_p=0.052	L_s=0.041
Width (m)	w_m=0.016	w_p=0.016	w_e=0.016
Thickness (μm)	h_m=250	h_p=48	h_s=18
Young's modulus (GPa)	E_m=117	E_p=3	E_s=5
Density (kg/m^3)	ρ_m=8960	ρ_p=1780	ρ_s=1820
Dielectric constant		ε_{33}^T =12	-
Piezo strain coefficient (C/N)		d_{31}=-23×10^{-12}	-
Capacitance (nF)		C_p=2.7	-

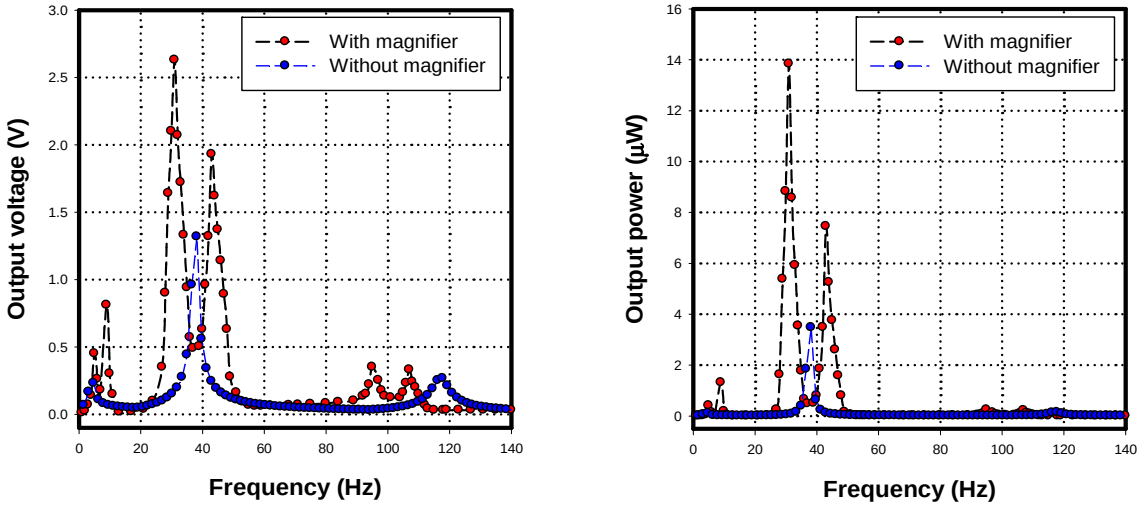

(a) (b)

Fig. 6. Experimental data of CPEH and EHDM at load resistance 500 kΩ of (a) output voltage, and (b) Output power versus frequency.

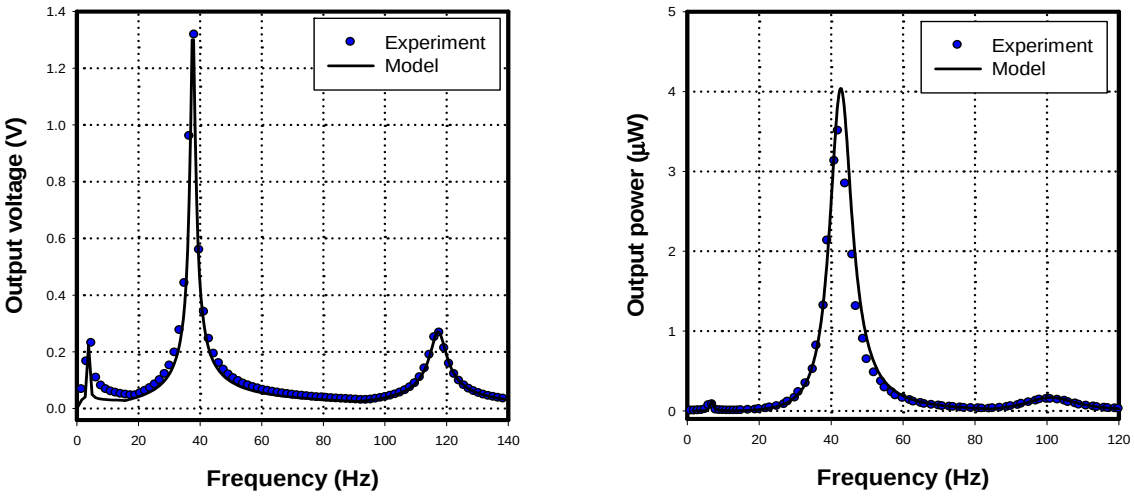

(a) (b)

Fig. 7. Experimental and theoretical data of (a) output voltage, and (b) output power versus frequency of CPEH at load resistance 500 kΩ.

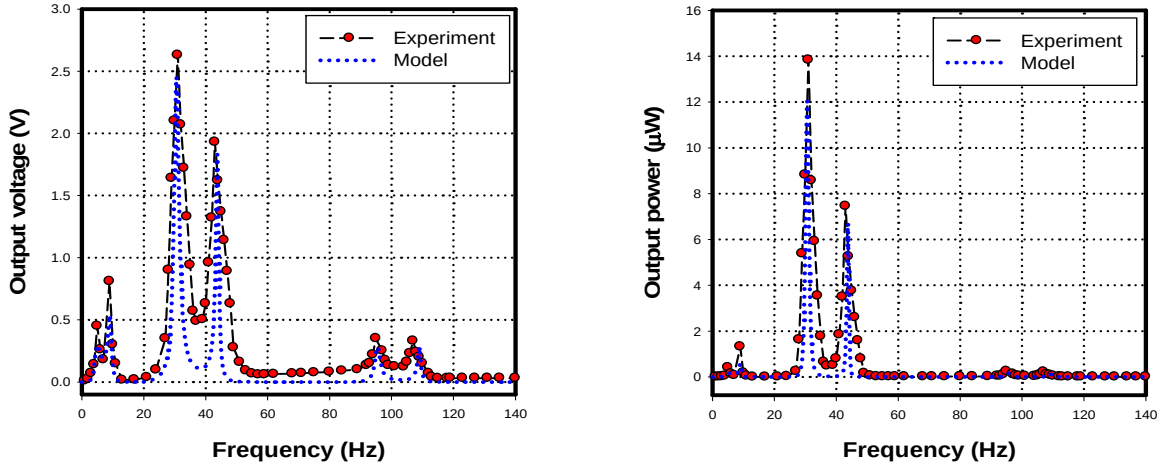

(a) (b)

Fig. 8. Experimental and theoretical data of (a) output voltage, and (b) output power versus frequency of EHDM at load resistance 500 kΩ.

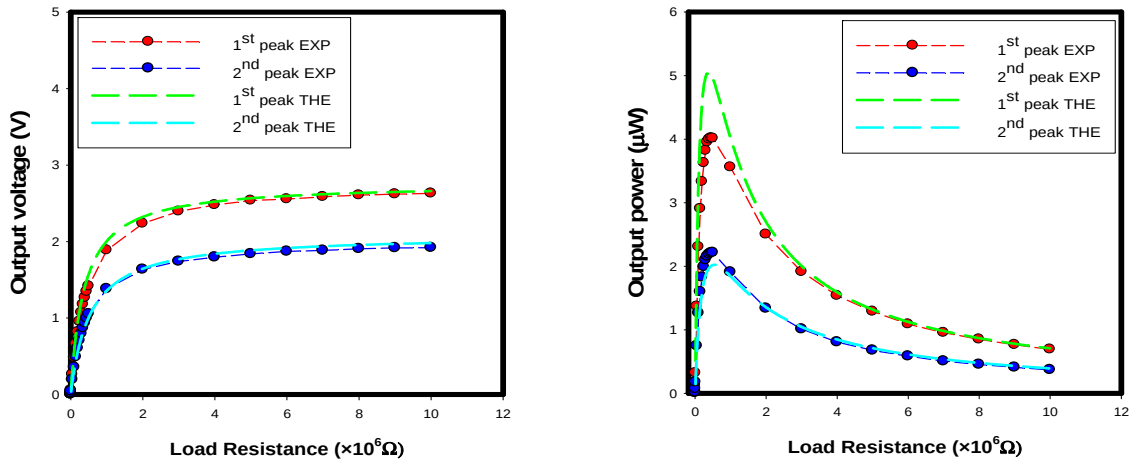

(a) (b)

Fig. 9. Experimental and theoretical data of (a) output voltage, and (b) output power versus load resistance of EHDM at second mode shape.

Table 2. Resonance frequency, voltage and power output parameters of CPEHM and EHDM.

Cantilever beam type and mode shape		Resonance frequency (Hz)			Output voltage (V)			Output power (μW)		
		EXP.	MAT.	Error (%)	EXP.	MAT.	Error (%)	EXP.	MAT.	Error (%)
CPEHM	First Mode	6.02	3.57	40.7	0.23	0.22	4.34	0.12	0.11	8.33
	Second Mode	37.42	36.90	1.39	1.32	1.30	1.51	3.48	3.39	2.58
	Third Mode	117.1	117.4	0.25	0.28	0.27	3.57	0.18	0.14	22.22
EHDM	First Mode	5.02	5.24	4.38	0.45	0.29	35.55	0.52	0.18	65.38
		8.69	8.96	3.11	0.82	0.53	35.36	1.35	0.43	68.15
	Second Mode	31.04	30.64	1.28	2.62	2.45	6.48	13.68	11.88	13.16
		42.72	43.76	2.43	1.92	1.81	5.72	7.47	6.54	12.45
	Third Mode	95.04	95.64	0.63	0.35	0.25	28.57	0.32	0.11	65.62
		107.3	109.2	1.77	0.33	0.25	24.24	0.27	0.18	33.33

4.2. Simulation and Analysis of EHDM Using MATLAb and COMSOL

By using Eq. (6) the displacement $u(x, t)$ of the uniphorm beam with magnifier can be obtained. The first three modes of CPEH system are shown in Fig. 10. Fig. 10(a) shows the theoretical results of model where the first three mode shapes happens approximately at 3.6 Hz, 37.5 Hz and 117.7 Hz, respectively. Fig. 10(b) shows the modeling results of CPEH using FEM where the first three mode shapes happens approximately at 9.3 Hz, 37.4 Hz and 108.4 Hz, respectively. Fig. 11 shows the theoretical results of EHDM using MATLAB R2015a, this figure indicates clearly that the dynamic magnifier energy harvester has an additional mode of vibration appearing at each resonance mode. For each mode, the first resonance (red line) is primarily due to the magnifier and the second resonance (blue line) is due to the unimorph beam [22].

For the more general case, FEM analysis is performed in COMSOL Multiphysics in two dimensions to investigate the resonance frequencies and modes of vibration of EHDM structure. As it is known the power density would be maximum when the vibration frequency matches the resonant frequency of piezoelectric harvester. A very fine mesh is used for generating accurate results of EHDM system. The natural frequencies and the corresponding mode shapes of EHDM of the first six mode shapes are shown in Fig. 12. The resonance frequency of each vibration mode in Fig. 10 – Fig. 12 are summarized in Table 3.

The columns in red line are represented an error between the measured, MATLAB and COMSOL data as can be seen in general, the percentage error in COMSOL or FEM is less than that calculated by MATLAB.

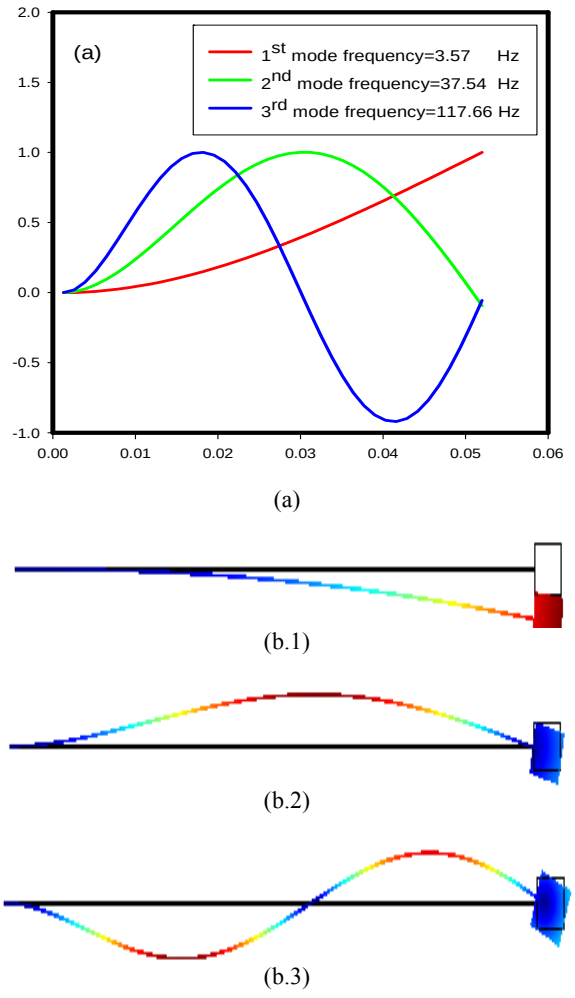

Fig. 10. The first three mode shapes of CPEH obtained from the (a) theoretical analysis (MATLAB R2015a), where the first mode is 3.57 Hz, second mode is 37.54 Hz, and third mode is 117.66 (b) COMSOL software, where (b.1) the first mode is 9.29 Hz, (b.2) second mode is 37.44 Hz, (b.3) third mode is 108.36.

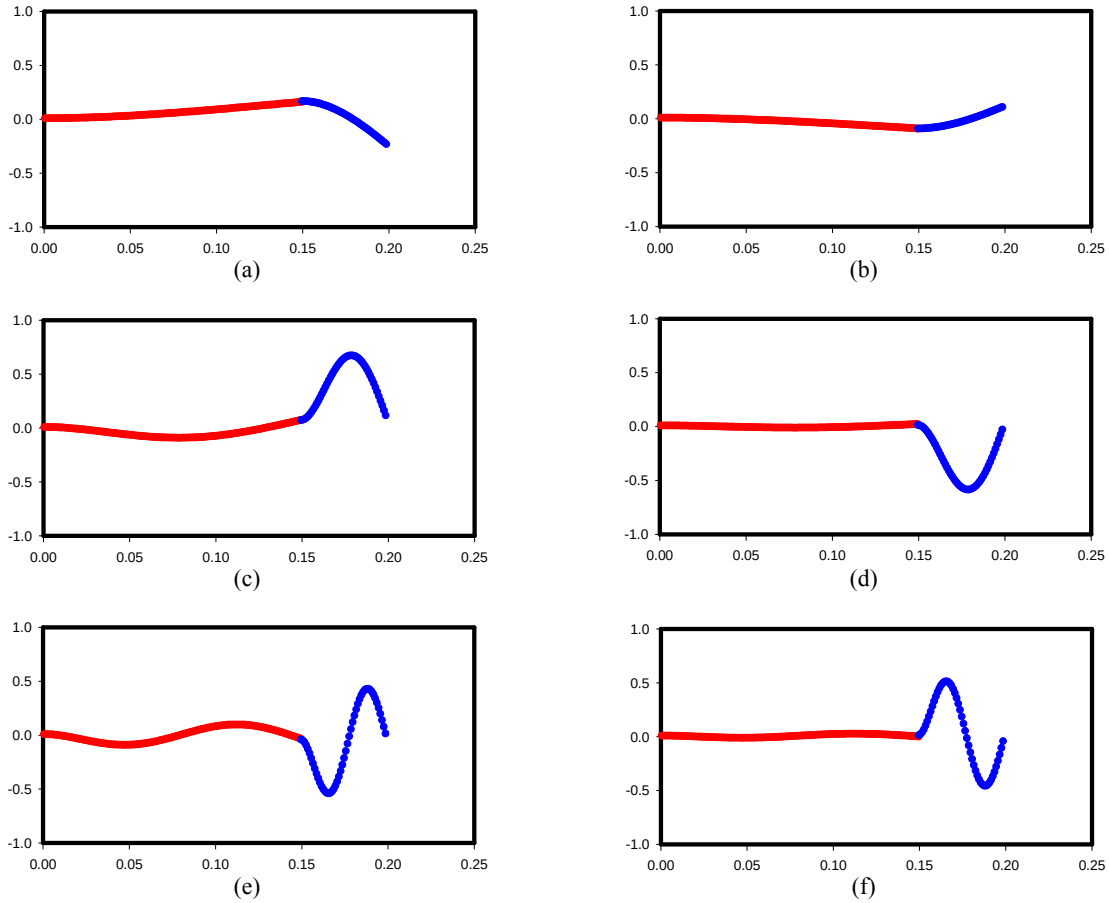

Fig. 11. The first six mode shapes of the EHDM structure obtained from the theoretical analysis (MATLAB R2015a), where the first resonance is mainly due to the magnifier and the second resonance is mainly due to the harvesting beam: (a) magnifier (fn = 3.58 Hz); (b) beam (fn = 6.81 Hz); (c) magnifier (fn = 30.95 Hz); (d) beam (fn = 42.69 Hz); (e) magnifier (fn = 95.08 Hz); (f) beam (fn = 119.54 Hz).

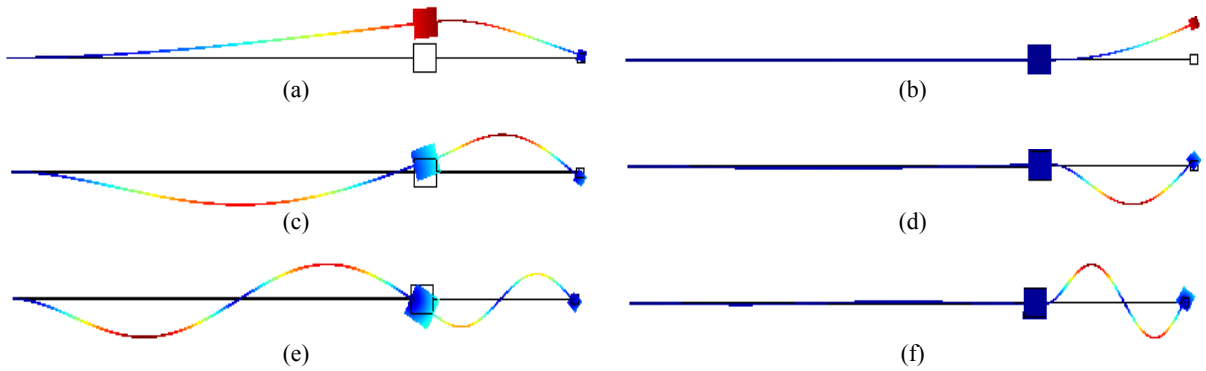

Fig. 12. The first six mode shapes of the EHDM structure obtained from the FEM (COMSOL 5.0), where the first resonance is mainly due to the magnifier and the second resonance is mainly due to the harvesting beam: (a) magnifier (fn = 4.07 Hz); (b) beam (fn = 7.65 Hz); (c) magnifier (fn = 30.99 Hz); (d) beam (fn = 44.45 Hz); (e) magnifier (fn = 95.21 Hz); (f) beam (fn = 130.76 Hz).

5. Conclusions

This paper has examined the effect of attaching a piezo-unimorph beam with tip mass on the output electrical parameters and bandwidth of a CPEH and EHDM at both an experimental and theoretical level. The experimental results show maximum output voltage generated by a conventional energy harvester at single frequency value of 37 Hz, where the maximum output voltage generated by EHDM are in frequency range of 31 Hz to 42 Hz. This result highlights the higher bandwidth of the EHDM compared to the CPEH and overlapping of modes of resonance of the system. The analytical model, which predicts the electrical parameters of this system is based on dividing the structure into elementary parts,

all these parts and proof mass have been written in the form of matrix representation with good agreement with the experimental data. The theoretical results of mode shapes of CPEH and EHDM have obtained and validated with MATLAB software and the FEM (COMSOL). The modeling approach provides a basis to design energy harvesters exploiting dynamic magnification for improved performance.

Table 3. Experimental, MATLAB and COMSOL resonance frequency results of EHDM.

Cantilever beam type and mode shape		Resonance frequency (Hz)				
		EXP.	MATLAB	Error (%)	COMSOL	Error (%)
CPEHM	First Mode	6.02	3.57	40.69	9.29	54.31
	Second Mode	37.42	37.54	0.32	37.44	0.05
	Third Mode	117.1	117.66	0.48	108.36	7.46
EHDM	First Mode	5.02	3.58	28.68	4.07	18.92
		8.69	6.81	21.63	7.65	11.96
	Second Mode	31.04	30.95	0.29	30.99	0.16
		42.72	42.69	0.07	44.45	4.05
	Third Mode	95.04	95.08	0.04	95.21	0.18
		107.3	119.54	11.40	130.76	21.86

Acknowledgements

The authors gratefully acknowledge support for this work through the National Science Foundation grant #EPSCoR R-II-3 (EPS-1158862). Authors thank Dr. Chance M. Glenn, Dean, College of Engineering, Technology and Physical Sciences and Dr. M. D. Aggarwal, Chairman, Department of Physics, Chemistry and Physics for their keen interest in this work. Authors thank Mr. Garland Sharp for fabrication of the sample holders.

References

[1]. J. Paradiso, T. Starner, Energy scavenging for mobile and wireless electronics, *IEEE Pervasive Computing,* Vol. 4, Issue 1, 2005, pp. 18-27.

[2]. H. Yu, J. Zhou, L. Deng, Z. Wen, A Vibration-Based MEMS Piezoelectric Energy Harvester and Power Conditioning Circuit, *Sensors*, Vol. 14, Issue 2, 2014, pp. 3323-3341.

[3]. X. Zhang, Active Omni-directional Piezoelectric Energy Harvesting System for Wireless Monitoring on Electrical Traction Shearer, *International Journal of Smart Home,* Vol. 8, Issue 3, 2014, pp. 19-32.

[4]. D. Shen, J.-H. Park, J. H. Noh, S.-Y. Choe, S.-H. Kim, H. C. Wikle, D.-J. Kim, Micromachined PZT cantilever based on SOI structure for low frequency vibration energy harvesting, *Sensors Actuators A: Physical*, Vol. 154, Issue 1, 2009, pp. 103-108.

[5]. M. Ferrari, V. Ferrari, M. Guizzetti, D. Marioli, A. Taroni, Piezoelectric multifrequency energy converter for power harvesting in autonomous microsystems, *Sensors Actuators A: Physical*, Vol. 142, Issue 1, 2008, pp. 329-335.

[6]. C. R. Bowen, H. A. Kim, P. M. Weaver, S. Dunn, Piezoelectric and ferroelectric materials and structures for energy harvesting applications, *Energy & Environmental Science,* Vol. 7, Issue 1, 2014, pp. 25-44.

[7]. J. Qiu, H. Ji, The Application of Piezoelectric Materials in Smart Structures in China, *International Journal of Aeronautical and Space Sciences,* Vol. 11, Issue 4, 2010, pp. 266-284.

[8]. H. Wu, L. Tang, Y. Yang, C. K. Soh, A novel two-degrees-of-freedom piezoelectric energy harvester, *Journal of Intelligent Material Systems and Structures,* Vol. 24, Issue 3, 2012, pp. 357-368.

[9]. Y. Ting, G. Hariyanto, B. K. Hou, S. Ricky, S. Amelia, C.-K. Wan, Investigation of Energy Harvest and Storage by Using Curve-shape Piezoelectric Unimorph, in *Proceedings of the IEEE International Symposium on Industrial Electronics (ISIE),* Seoul, South Korea, 2009, pp. 2047-2052.

[10]. J. W. Xu, W. W. Shao, F. R. Kong, Z. H. Feng, Right-angle piezoelectric cantilever with improved energy harvesting efficiency, *Applied Physics Letters*, Vol. 96, Issue 15, 2010, 152904.

[11]. A. Erturk, J. M. Renno, D. J. Inman, Modeling of Piezoelectric Energy Harvesting from an L-Shaped Beam-Mass Structure with an Application to UAVs, *Journal of Intelligent Material Systems and Structures,* Vol. 20, Issue 5, 2009, pp. 529-544.

[12]. N. A. Kong, D. S. Ha, A. Etrurk, D. J. Inman, Resistive impedance matching circuit for piezoelectric energy harvesting, *Journal of Intelligent Material Systems and Structures,* Vol. 21, Issue 13, 2010, pp. 293-302.

[13]. J. Liang, W.-H. Liao, Impedance matching for improving piezoelectric energy harvesting systems, in *Proceedings of the SPIE Int. Conf. Active and Passive Smart Struct. Intell. Syst.,* San Diego, CA, USA, Vol. 7643, 2010.

[14]. W. J. Wu, Y. Y. Chen, B. S. Lee, J. J. He, Y. T. Pen, Tunable resonant frequency power harvesting devices, in *Proceedings of the SPIE Int. Conf. Smart Struct. Mater. Damping and Isolation.,* San Diego, CA, USA, Vol. 6169, 2006.

[15]. A. Badel, D. Guyomar, E. Lefeuvre, C. Richard, Piezoelectric energy harvesting using a synchronized switch technique, *Journal of Intelligent Material Systems and Structures,* Vol. 17, Issue 8-9, 2006, pp. 831-839.

[16]. X. Tang, L. Zuo, Enhanced vibration energy harvesting using dual-mass systems, *Journal of Sound and Vibration*, Vol. 330, Issue 21, 2011, pp. 5199-5209.

[17]. V. K. Sharma, K. Srikanth, A. K. Viswanath, Influence of cross-sectional area of a dynamic magnifier for vibration energy harvesting, *International Journal of Mechanical and Production Engineering*, Vol. 2, Issue 5, 2014, pp. 82-85.

[18]. W. Zhou, G. R. Penamalli, L. Zuo, An efficient vibration energy harvester with a multi-mode dynamic magnifier, *Smart Materials and Structures*, Vol. 21, Issue 1, 2012, 015014.

[19]. A. Aladwani, M. Arafa, O. Aldraihem, A. Baz. Cantilevered piezoelectric energy harvester with a dynamic magnifier, *Journal of Vibration and Acoustics*, Vol. 134, Issue 3, 2012, pp. 031004-1–031004-10.

[20]. O. Aldraihem, A. Baz, Energy harvester with a dynamic magnifier, *Journal of Intelligent Material Systems and Structures,* Vol. 22, Issue 6, 2011, pp. 521-530.

[21]. S. B. Lee, B. D. Youn, B. C. Jung, Robust Segment-Type Energy Harvester and Its Application to a Wireless Sensor, *Smart Materials and Structures*, Vol. 18, Issue 9, 2009, pp. 095021-1–095021-12.

[22]. D. Vasic, F. Costa, Modeling of Piezoelectric Energy Harvester with Multi-mode Dynamic Magnifier with Matrix Representation, *International Journal of Applied Electromagnetics and Mechanics*, Vol. 43, Issue 3, 2013, pp. 237-255.

[23]. S.-L. Kok, Design, Fabrication and Characterization of Free Standing Thick-Film Piezoelectric Cantilevers for Energy Harvesting, *University of Southampton,* 2013.

[24]. H. Porwal, Piezoelectric Transduction Mechanism for Vibration Based Energy Harvesting, Master Thesis, *National Institute of Technology,* Rourkela, India, 2013.

[25]. R. Patel, Modelling, Analysis and Optimization of Cantilever Piezoelectric Energy Harvesters, Doctoral *Dissertation*, *University* of *Nottingham*, Nottingham, 2012.

[26]. J. R. Davidson, C. Mo, Piezoelectric Energy Harvesting with Frequency Tuning for Ventilation System Monitoring, *International Journal of Engineering Science and Innovative Technology*, Vol. 2, Issue 5, 2013, pp. 114-124.

[27]. Y. S. Cho, Y. E. Pak, C. S. Han, S. K. Ha, Five-port equivalent electric circuit of piezoelectric bimorph beam, *Sensors Actuators A: Physical,* Vol. 84, Issue 1-2, 2000, pp. 140-148.

[28]. A. Erturk, Electromechanical Modeling of Piezoelectric Energy Harvesters, PhD Thesis, *Virginia Polytechnic Institute and State University*, 2009.